THE JOURNAL OF BIOLOGICAL CHEMISTRY VOL. 290, NO. 2, pp. 960–971, January 9, 2015

Heterozygous Null Bone Morphogenetic Protein Receptor Type 2 Mutations Promote SRC Kinase-dependent Caveolar Trafficking Defects and Endothelial Dysfunction in Pulmonary Arterial Hypertension*

Received for publication, June 20, 2014, and in revised form, November 18, 2014 Published, JBC Papers in Press, November 19, 2014, DOI 10.1074/jbc.M114.591057

Allison R. Prewitt[‡1,2], **Sampa Ghose**[§1], **Andrea L. Frump**[‡], **Arumima Datta**[§], **Eric D. Austin**[¶], **Anne K. Kenworthy**[‖], **and Mark P. de Caestecker**[§3]

From the Departments of [‡]*Cell and Developmental Biology,* [§]*Medicine,* [¶]*Pediatrics, and* [‖]*Molecular Physiology and Biophysics, Vanderbilt University, Nashville, Tennessee 37232*

Background: Hereditary pulmonary arterial hypertension (HPAH) is a lethal disease associated with bone morphogenetic protein receptor 2 (*BMPR2*) mutations.
Results: *Bmpr2*$^{+/-}$ mutant mice and HPAH patient endothelial cells have SRC-mediated caveolar trafficking defects and endothelial dysfunction.
Conclusion: SRC-dependent caveolar trafficking defects may contribute to the development of HPAH.
Significance: This work suggests new therapeutic targets for the treatment of HPAH.

Hereditary pulmonary arterial hypertension (HPAH) is a rare, fatal disease of the pulmonary vasculature. The majority of HPAH patients inherit mutations in the bone morphogenetic protein type 2 receptor gene (*BMPR2*), but how these promote pulmonary vascular disease is unclear. HPAH patients have features of pulmonary endothelial cell (PEC) dysfunction including increased vascular permeability and perivascular inflammation associated with decreased PEC barrier function. Recently, frameshift mutations in the caveolar structural protein gene Caveolin-1 (CAV-1) were identified in two patients with non-*BMPR2*-associated HPAH. Because caveolae regulate endothelial function and vascular permeability, we hypothesized that defects in caveolar function might be a common mechanism by which *BMPR2* mutations promote pulmonary vascular disease. To explore this, we isolated PECs from mice carrying heterozygous null *Bmpr2* mutations (*Bmpr2*$^{+/-}$) similar to those found in the majority of HPAH patients. We show that *Bmpr2*$^{+/-}$ PECs have increased numbers and intracellular localization of caveolae and caveolar structural proteins CAV-1 and Cavin-1 and that these defects are reversed after blocking endocytosis with dynasore. SRC kinase is also constitutively activated in *Bmpr2*$^{+/-}$ PECs, and localization of CAV-1 to the plasma membrane is restored after treating *Bmpr2*$^{+/-}$ PECs with the SRC kinase inhibitor 3-(4-chlorophenyl)-1-(1,1-dimethylethyl)-1*H*-pyrazolo[3,4-*d*]pyrimidin-4-amine (PP2). Late outgrowth endothelial progenitor cells isolated from HPAH patients show similar increased activation of SRC kinase. Moreover, *Bmpr2*$^{+/-}$ PECs have impaired endothelial barrier function, and barrier function is restored after treatment with PP2. These data suggest that heterozygous null *BMPR2* mutations promote SRC-dependent caveolar trafficking defects in PECs and that this may contribute to pulmonary endothelial barrier dysfunction in HPAH patients.

Pulmonary arterial hypertension (PAH)[4] is a progressive disease of the lung vasculature characterized by sustained elevation in pulmonary arterial pressures leading to right ventricular failure. Current therapy for patients with PAH improves exercise tolerance and hemodynamics, but survival benefits are limited (1). Importantly, none of these treatments are directed against the underlying cause of this disease. For this reason, there was considerable enthusiasm in the field over a decade ago when mutations in the BMP family receptor *BMPR2* were discovered in patients with a rare, autosomal dominant form of the disease known as hereditary pulmonary arterial hypertension (HPAH) (2). Since that time *BMPR2* mutations have been identified in ~75% of patients with a family history of PAH and ~25% of those with apparently sporadic disease (3). The majority of these mutations are inactivating, null mutations. There is also increasing evidence that patients with other forms of PAH that are not associated with *BMPR2* mutations have reduced BMPR2 expression (4–6), suggesting that defective BMPR2 signaling and/or expression contributes to the pathogenesis of pulmonary vascular disease. Despite these findings there is no

* This work was supported, in whole or in part, by National Institutes of Health Grants R01HL093057 (to M. P. d. C.), R01HL111259 (to A. K. K.), and R03HL115112 (to M. P. d. C.).
[1] Both authors contributed equally to this work.
[2] Supported by American Heart Association Predoctoral Fellowship 12PRE11900020.
[3] To whom correspondence should be addressed: Dept. of Medicine Division of Nephrology, Vanderbilt University Medical Center, 1161 21st Ave. S., S3223 Medical Center North, Nashville, TN 37232. Tel.: 615-343-2844; Fax: 615-343-2675; E-mail: mark.de.caestecker@vanderbilt.edu.

[4] The abbreviations used are: PAH, pulmonary arterial hypertension; BMP, bone morphogenetic protein; BMPR2, bone morphogenetic protein type 2 receptor; HPAH, hereditary pulmonary arterial hypertension; PEC, pulmonary endothelial cell; CAV-1, Caveolin-1; LO-EPC, late outgrowth endothelial progenitor cell; PP2, 3-(4-chlorophenyl)-1-(1,1-dimethylethyl)-1*H*-pyrazolo[3,4-*d*]pyrimidin-4-amine; PP3, 4-amino-7-phenylpyrazol[3,4-*d*]pyrimidine; TEER, transendothelial electrical resistance; ANOVA, analysis of variance.

clear consensus as to how BMPR2 signaling defects promote pulmonary vascular dysfunction in patients with PAH (7).

The pulmonary endothelium may be the primary target of vascular injury in HPAH patients because it expresses high levels of BMPR2 (4, 8–10). Heterozygous *Bmpr2* mutant mice have pulmonary endothelial cell (PEC) dysfunction with decreased endothelium-dependent relaxation in isolated intrapulmonary pulmonary artery preparations (8). In addition, mice with conditional deletion of *Bmpr2* in the endothelium develop spontaneous pulmonary hypertension and have endothelial barrier dysfunction associated with increased pulmonary vascular leak and perivascular inflammation (11–13). Increased perivascular inflammation also occurs in patients with pulmonary hypertension (14–16). These data suggest that endothelial dysfunction associated with abnormal endothelium-dependent vasodilatation and with decreased endothelial barrier function contributes to pulmonary vascular pathophysiology in patients with HPAH.

Caveolae are specialized plasma membrane microdomains that form 50–100-nm flask-shaped invaginations of the plasma membrane (17). Core caveolar structural proteins Caveolins and Cavins regulate the structure, trafficking, and function of these microdomains. Caveolae are widely expressed in most cell types but are markedly enriched in endothelial cells where they play a critical role in regulating endothelial function and permeability (18–20). In the pulmonary vasculature, loss of Caveolin-1 (CAV-1) expression promotes pulmonary hypertension in mice (21) and is associated with chronic activation of endothelial NOS that results in enhanced pulmonary vasoconstriction (22). Additionally, caveolar numbers are deregulated in the pulmonary vasculature of patients with idiopathic PAH (23), and recent studies have identified *BMPR2*-negative HPAH patients with frameshift mutations in the *CAV-1* gene (24, 25). These data suggest that caveolar defects can promote pulmonary vascular disease, but the relationship between caveolae and the pathogenesis of *BMPR2* mutation-associated HPAH has not been established.

In these studies, we have used PECs derived from heterozygous null $Bmpr2^{+/-}$ mutant mice to establish that loss of a single *Bmpr2* allele gives rise to enhanced, SRC kinase-dependent caveolar trafficking. Late outgrowth endothelial progenitor cells (LO-EPCs) isolated from the peripheral blood of an HPAH patient have a similar defect in SRC activation. We also show that $Bmpr2^{+/-}$ mutant PECs have decreased barrier function and that treatment with a SRC kinase inhibitor reverses the caveolar trafficking defect and reduces permeability in $Bmpr2^{+/-}$ PECs. These data establish for the first time a relationship between *BMPR2* mutations and caveolar trafficking defects that may promote pulmonary vascular disease in HPAH and suggest that SRC kinase inhibitors may be used therapeutically to ameliorate these effects.

EXPERIMENTAL PROCEDURES

Chemicals and Reagents—Recombinant human BMP2 (R&D Systems); 3-(4-chlorophenyl)-1-(1,1-dimethylethyl)-1*H*-pyrazolo-[3,4-*d*]pyrimidin-4-amine (PP2) (Cayman Chemical); dynasore hydrate, 70-kDa dextran-rhodamine, and FITC-conjugated albumin, SKI606 (bosutinib) (Sigma-Aldrich); Alexa Fluor 555-albumin, Alexa Fluor 488-concanavalin A (Molecular Probes); interferon γ (IFNγ) (Peprotech); Dio-Ac-LDL (Biomedical Technologies Inc); and PP3 (Millipore) were from the indicated sources. Monoclonal antibodies include $Tyr(P)^{14}$-CAV-1 (clone 56), CAV-1 (clone 2234), BMPR2 (clone 18), β-catenin (clone 14) (BD Biosciences), and β-actin (clone AC-74) (Sigma). Polyclonal antibodies include CAV-1, $Tyr(P)^{416}$-SRC, and SRC (Cell Signaling Technology) and Cavin-1 (Bethyl Laboratories). Antibodies for fluorescence-activated cell sorting (FACS) analysis include CD31 (clone WM59), CD146 (clone P1H12), CD14 (M5E2), and CD45 (clone HI30) (BD Biosciences).

Mouse Pulmonary Endothelial Cell (PEC) Isolation, Characterization, and Culture—Six independent lines of PECs were generated from three wild-type (W1, W2, and W3) and three $Bmpr2^{\Delta ex4\text{-}5/+}$ ($Bmpr2^{+/-}$) (N1, N3, and N6) mice (26) as described above. For this, $Bmpr2^{+/-}$ mice were maintained on a C57Bl/6 background (>10 generations backcrossed) and crossed with C57Bl/6 H-2Kb-tsA58 SV40 large T antigen transgenic mice (Charles Rivers "immortomice") to generate wild-type and $Bmpr2^{+/-}$ immortomice. Genotype was confirmed by PCR using primers and conditions outlined in previous studies (27, 28). To isolate PECs, mice were anesthetized with isoflurane prior to sacrifice by cervical dislocation. Lungs were perfused with a mixture of phosphate-buffered saline (PBS) and 2 mM EDTA followed by 0.25% trypsin, 2 mM EDTA via right ventricle. Heart and lungs were removed en bloc and incubated at 37 °C for 20 min. Finally, lungs were perfused again in complete endothelial microvascular medium EGM-2MV (Lonza), and the perfusate was recovered for isolated cells. Cells were grown under permissive conditions in EGM-2MV + 10 units/ml INFγ at 33 °C before being transferred to 37 °C without INFγ for 3–5 days to inhibit SV40 large T antigen activity for phenotyping and before conducting experiments. Endothelial cell phenotype was confirmed for all isolates by >90% vascular cell adhesion molecule- and endothelial protein C receptor-positive expression by FACS using mouse anti-vascular cell adhesion molecule-Alexa Fluor 647 (clone 429) and endothelial protein C receptor-allophycocyanin (clone eBio1560) (eBioscience) and by the ability to form tubes in three-dimensional culture in collagen I as described (28, 29). For PP2 treatment, experiments were performed in complete medium. Dynasore treatment was performed in serum-free basal EBM2 medium. For BMP2 treatment, cells were first serum-starved in basal EBM2 medium with 0.1% bovine serum albumin (Sigma) for 18 h.

Isolation and Characterization of LO-EPCs—LO-EPCs were isolated from peripheral blood samples as described previously (30). Roughly 60 ml of blood was collected from each patient and aliquoted into 50-ml Falcon tubes containing 3 ml of 3.8% sodium citrate. Samples were collected from normal volunteers and PAH patients attending the Vanderbilt Pulmonary Hypertension Clinic after obtaining informed consent under a Vanderbilt University Institutional Review Board-approved protocol (Institutional Review Board number 9401 "Genetic and Environmental Pathogenesis of PPH"). The blood was then diluted 1:1 with PBS and slowly layered atop 10 ml of Ficoll (GE Healthcare) in a separate tube. Samples were then spun at

400 × *g* for 35 min at room temperature with brake and accelerator turned off. The mononuclear cell layer was then collected from the Ficoll density gradient and diluted 1:1 in PBS followed by centrifugation for 20 min at 300 × *g* at room temperature. The supernatant was discarded, and the cell pellet was resuspended in EGM-2MV + 20% ES cell grade fetal bovine serum (FBS; Hyclone). The cell suspension was then plated into T-75 flasks coated with 5 μg/cm^2 collagen I (BD Biosciences). Medium was changed every 2 days, and LO-EPC colonies were pooled 2–3 weeks after plating as described (30). Endothelial cell phenotype was confirmed by Dio-Ac-LDL uptake and by flow cytometry for the presence of endothelial cell markers CD31 and CD146 and the absence of leukocyte and macrophage markers CD45 and CD14, respectively. Briefly, cells were plated on gelatin-coated coverslips before being incubated in 10 μg/ml Dio-Ac-LDL for 4 h at 37 °C. Cells were then rinsed in PBS and fixed in 4% paraformaldehyde for imaging. For FACS, cells were trypsinized and centrifuged, and cell pellets were resuspended in 100 μl of EGM-2 basal serum with the desired antibody. After incubation on ice for 1 h, samples were centrifuged, resuspended in basal EGM-2 medium, and evaluated by FACS using a BD FACSCanto II system.

Characterization of Caveola Numbers—For transmission electron microscopy, PECs were fixed in 2.5% glutaraldehyde and 0.1 M sodium cacodylate prior to ethanol dehydration. Cells were subsequently pelleted by gravity in propylene oxide and embedded in resin for imaging on a Philips FEI T-12 transmission electron microscope. For tissue fixation, we performed tracheal perfusion with the same fixative. Total PEC caveolae were counted in three randomly selected images per mouse lung. Caveola numbers were quantified by a blinded observer counting caveola-like structures of 50–100-nm size per micrometer of endothelial plasma membrane.

CAV-1 and Cavin-1 Localization in Isolated PECs—PECs were grown to confluence in non-permissive conditions on gelatin-coated coverslips. Cells were then fixed in 4% paraformaldehyde (Electron Microscopy Sciences) and permeabilized in 0.2% saponin (Sigma) in PBS at room temperature. Coverslips were incubated in primary antibody in 3% donkey serum in PBS overnight at 4 °C followed by secondary antibody for 1 h at room temperature. Nuclei were stained with Topro3 (Molecular Probes). Digital images were obtained by confocal microscopy using a Zeiss LSM510-Meta microscope. To quantify subcellular localization of CAV-1 and Cavin-1, horizontal digital slices were taken across the middle of each cell, and immunofluorescence localization of CAV-1 and Cavin-1 was quantified by generating intensity plots using the ImageJ software "plot profile" function. To correct for differing cell size during fluorescent quantification, the distance across the cell was normalized to 100 arbitrary units. Intensity of CAV-1 and Cavin-1 fluorescence at the plasma membrane was quantified by averaging the fluorescence intensity of the first and last 20 distance units and dividing by the average intensity of the middle 21–79 distance units. We evaluated between 10 and 30 cells for each cell line under each condition, pooling results for each genotype or treatment condition, as indicated in the figure legends. Serial z-stack sections were also gathered at the time of analysis and reconstructed using LSM510 software to evaluate the intracellular distribution of CAV-1.

Western Blotting—Cells were lysed in 1× lysis buffer containing 150 mM NaCl, 25 mM HEPEs, 5 mM EDTA, 1% Triton X-100, 10% glycerol, and phosphatase and protease inhibitors (1:100; Sigma) on ice for 15 min before centrifugation at 5000 × *g* for 30 min. Western blots were blocked in 5% milk before incubation in primary antibody in either 5% milk or bovine serum albumin (BSA) for phosphorylation site-specific antibodies overnight at 4 °C. Primary antibodies were detected using species-specific HRP-conjugated secondary antibodies and PerkinElmer Western Lightning Plus ECL reagent. Films were exposed over a range of times and digitally scanned, and densitometry was performed using ImageJ on films exposed for intermediate time periods to avoid non-linear ECL signals associated with very short or long exposure times.

Albumin Endocytosis in Isolated PECs—Cells were grown to confluence in non-permissive conditions on gelatin-coated coverslips in complete EGM-2MV medium before being switched to basal EGM-2 medium immediately prior to the start of the experiment. Cells were incubated with or without dynasore for 30 min at 37 °C prior to the addition of 1 mg/ml Alexa Fluor 555-albumin in chilled basal EGM-2. Cells were then incubated at 4 °C for 30 min to inhibit endocytosis (31–33) while allowing fluorophore attachment before being transferred to 37 °C for 5 min to initiate endocytosis. Cells were then placed on ice and stripped of all membrane-bound fluorophore by three rounds of acid stripping in 100 mM glycine, pH 2.0 followed by Hanks' balanced salt solution, pH 7.4 each for 5 min on ice. Cells were then transferred to 37 °C for 10 s in Hanks' balanced salt solution, pH 7.4 to remove any remaining fluorophore. Immediately afterward cells were washed two times in PBS and fixed in 4% paraformaldehyde. Following fixation, cells were processed for confocal imaging.

Albumin Exocytosis in Isolated PECs—Cells were grown to confluence in non-permissive conditions on gelatin-coated coverslips in complete EGM-2MV medium. Cells were incubated in chilled medium containing 1 mg/ml Alexa Fluor 555-albumin and subsequently placed at 4 °C for 30 min to allow fluorophore binding. Cells were then transferred to 37 °C for 5 min to initiate endocytosis. Following endocytosis, cells were immediately incubated on ice and underwent one round of acid stripping (100 mM glycine, pH 2.0 followed by Hanks' balanced salt solution, pH 7.4 for 5 min each) to remove fluorophore bound to the cell surface. Cells were rinsed twice in PBS before addition of complete medium. The time 0 sample was collected at this point and placed on ice, and the remaining dishes were returned to 37 °C to allow exocytosis of the remaining internalized fluorophore. Cells were placed on ice at the indicated time points before undergoing two final rounds of acid stripping and subsequent fixation in 4% paraformaldehyde.

Endothelial Permeability—Transwell filters, 12 mm in size with 0.4-μm pore size, were coated in 0.1% gelatin in PBS and further prepared according to the manufacturer's recommendations. PECs were plated and grown to confluence in EGM-2MV on these filters for 3–4 days at 37 °C prior to treatment. Transendothelial electrical resistance (TEER) was tracked throughout the experiment using an EVOM2 voltmeter and

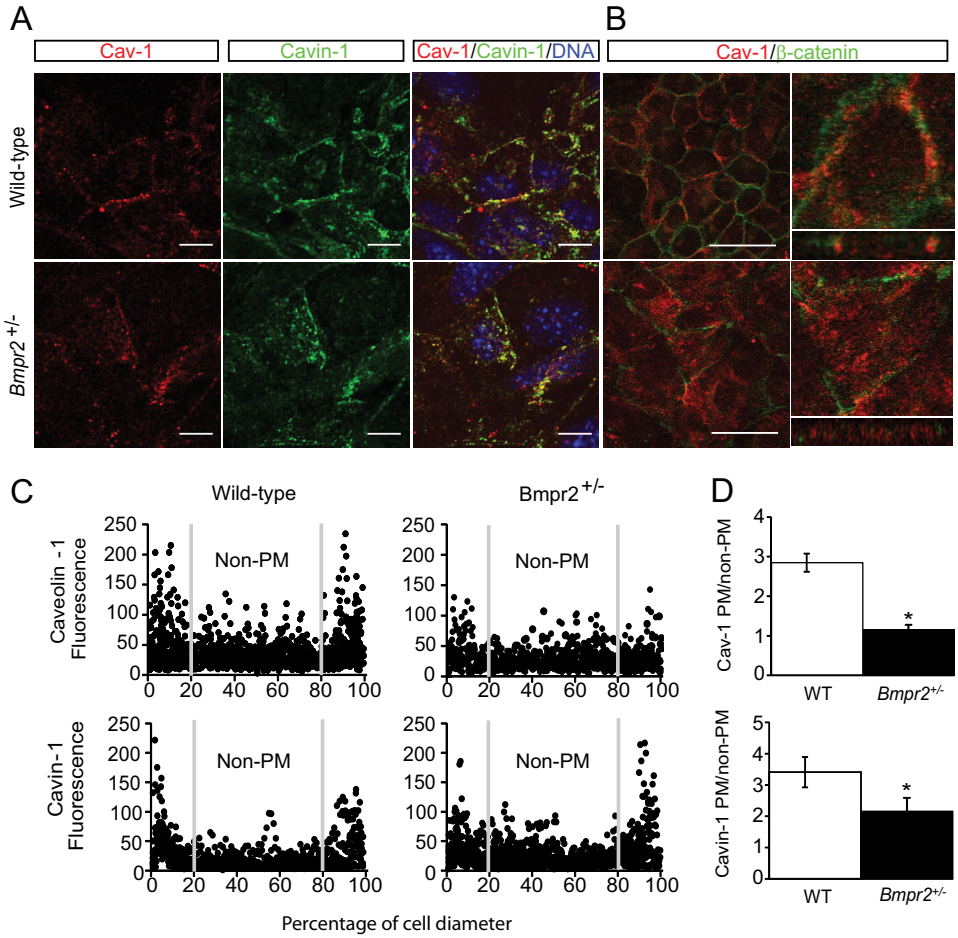

FIGURE 1. **Mislocalization of caveolar structural proteins in *Bmpr2*$^{+/-}$ PECs.** *A*, representative immunofluorescence images of CAV-1 (*red*) and Cavin-1 (*green*) in wild-type and *Bmpr2*$^{+/-}$ PECs. *Scale bars*, 10 μm. *B*, *left panels*, single *x*/*y* plane from z-stack images. Caveolin-1 (*red*) and β-catenin (*green*). *Scale bars*, 50 μm. *Right panels*, orthogonal views reconstructed from z-stack images depicting Caveolin-1 localization in *x*/*z* and *y*/*z* planes of a single cell magnified from the *left panels*. *C*, fluorescence intensity plots depicting CAV-1 and Cavin-1 distribution across the cells. *Gray lines* delineate plasma membrane (*PM*) from non-plasma membrane. Plots were generated from multiple cells from three wild-type ($n = 12$) and three *Bmpr2*$^{+/-}$ ($n = 14$) cell lines. Fluorescence is in arbitrary units, and distance is in percentage of cell diameter. *D*, quantitative analysis of CAV-1 and Cavin-1 localization. Values are expressed as the mean ratio of plasma membrane to non-plasma membrane fluorescence intensities. *Error bars* represent S.E. *, $p < 0.05$ *versus* wild-type controls (*t* test).

STX2 electrode (World Precision Instruments, *Inc.*). Permeability assessments began once TEER measurements plateaued. FITC-albumin (10 mg/ml) and 70-kDa rhodamine-dextran (1 mg/ml) were added to the upper chamber, and complete medium without additional fluorophores was added to the lower chamber. For parallel 4 °C/37 °C studies, cells were grown to confluence in EGM-2MV medium and transferred to 4 °C 30 min prior to fluorophore addition to block endocytosis (31–33). Samples were taken from the lower chamber at specified time points, and FITC-albumin and rhodamine-dextran were measured on the Molecular Probes SpectraMax at 488-nm emission/530-nm excitation and 570-nm emission/590-nm excitation, respectively. Studies were performed using one to three wild-type and *Bmpr2*$^{+/-}$ PEC lines as indicated in the figure legends and repeated in triplicate for each line.

Statistical Analyses—Statistical analyses were performed by Student's *t* test for paired group comparisons or one-way or two-way analysis of variance for multiple between group comparisons using Dunnett's or Šidák's correction for multiple post hoc between group comparisons as indicated. The minimal level of significance was set at $p < 0.05$. Statistical analyses were performed using GraphPad Prism 5 software.

RESULTS

Altered CAV-1 and Cavin-1 Localization in Bmpr2$^{+/-}$ *PECs*—To evaluate the effects of heterozygous *Bmpr2* mutations on caveolar localization and function in PECs, we first isolated and characterized six separate lines of conditionally immortalized PECs from three wild-type mice and three mice carrying heterozygous null *Bmpr2* mutations (*Bmpr2*$^{+/-}$ mice). When cultured under non-permissive temperatures, all six of these cell lines have typical endothelial cobblestone morphology and rapidly form tubelike structures in three-dimensional cultures, and >90% express the endothelium-specific markers *vascular cell adhesion molecule* and endothelial protein C receptor as assessed by FACS. These cells are advantageous over primary cultured endothelial cells because they can be maintained and expanded over numerous passages at permissive temperatures but redifferentiate and express endothelium-specific markers at non-permissive temperatures (8, 28, 29). Using these cells we show that there is altered localization of CAV-1 and Cavin-1 in *Bmpr2*$^{+/-}$ PECs from a predominantly plasma membrane localization in wild-type PECs to an intracellular localization in *Bmpr2*$^{+/-}$ PECs (Fig. 1). This is apparent both from represent-

ative immunofluorescence images (Fig. 1*A*) and from fluorescence intensity plots obtained across multiple PECs lines isolated from wild-type and *Bmpr2*$^{+/-}$ mice (Fig. 1*C*). Quantitative analysis of these fluorescence intensity plots confirms that there is a significant reduction in CAV-1 and Cavin-1 localization at the plasma membrane in *Bmpr2*$^{+/-}$ PECs (Fig. 1*D*). This effect is not associated with a change in cell shape or size as shown in orthogonal slices constructed from serial z-stacks of the entire cell (Fig. 1*B*) and is not associated with a generalized defect in plasma membrane markers because the adherens junction marker β-catenin was similarly membrane-localized in both wild-type and *Bmpr2*$^{+/-}$ PECs (Fig. 1*B*). Taken together, these data indicate that there is an increase in intracellular localization of CAV-1 and Cavin-1 in *Bmpr2*$^{+/-}$ PECs.

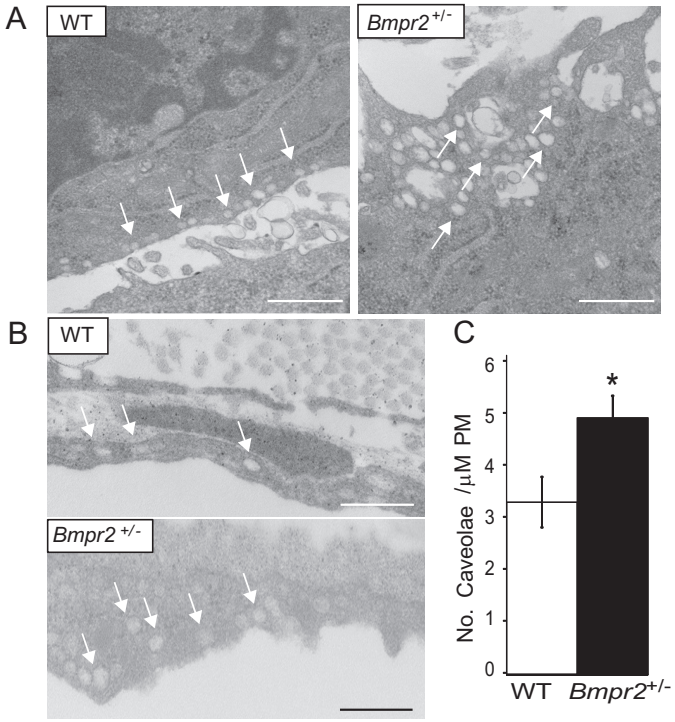

FIGURE 2. **Increased caveolar structures in *Bmpr2*$^{+/-}$ PECs and lungs.** *A*, transmission electron microscopy of cultured PECs from wild-type and *Bmpr2*$^{+/-}$ mice. *Arrows* indicate caveolar structures. *B*, transmission electron microscopy of lung sections from wild-type and *Bmpr2*$^{+/-}$ mice. *Arrows* indicate caveolar structures in the endothelium. *Scale bars*, 500 nm. *C*, quantitative analysis of caveolar structures in the lung endothelium from wild-type and *Bmpr2*$^{+/-}$ mice (five mice per group/three images per mouse). Values are expressed as the number of caveolae/μm of endothelium. *Error bars* represent S.E. *, $p < 0.01$ *versus* wild-type controls (*t* test). *PM*, plasma membrane.

Increased Number of Caveolae in Bmpr2$^{+/-}$ *Mouse Lungs and PECs*—We used transmission electron microscopy to determine whether changes in CAV-1 and Cavin-1 localization are associated with alterations in caveolar structures in *Bmpr2*$^{+/-}$ mouse PECs. There are increased numbers of intracellular caveola-like structures in PECs from *Bmpr2*$^{+/-}$ mice (Fig. 2*A*). Quantitative analysis of caveolar numbers in lung sections indicates that there are also increased numbers of caveola-like structures in the intact pulmonary endothelium of *Bmpr2*$^{+/-}$ mice (Fig. 2, *B* and *C*). These data indicate that changes in intracellular localization of CAV-1 and Cavin-1 are associated with increased numbers and intracellular localization of caveolae in *Bmpr2*$^{+/-}$ PECs.

Dynamin-2 Inhibition Restores CAV-1 Localization to the Plasma Membrane—Increased numbers of intracellular caveolae may result from enhanced Dynamin-2-mediated caveolar scission and endocytosis (34). We therefore evaluated the effect of dynasore, a selective cell-permeable Dynamin-2 inhibitor (35, 36), on CAV-1 localization in *Bmpr2*$^{+/-}$ PECs. Dynasore restores CAV-1 localization to the plasma membrane in *Bmpr2*$^{+/-}$ PECs (Fig. 3, *A* and *B*). These data suggest that increased intracellular localization of CAV-1 in *Bmpr2*$^{+/-}$ PECs results from increased caveolar endocytosis.

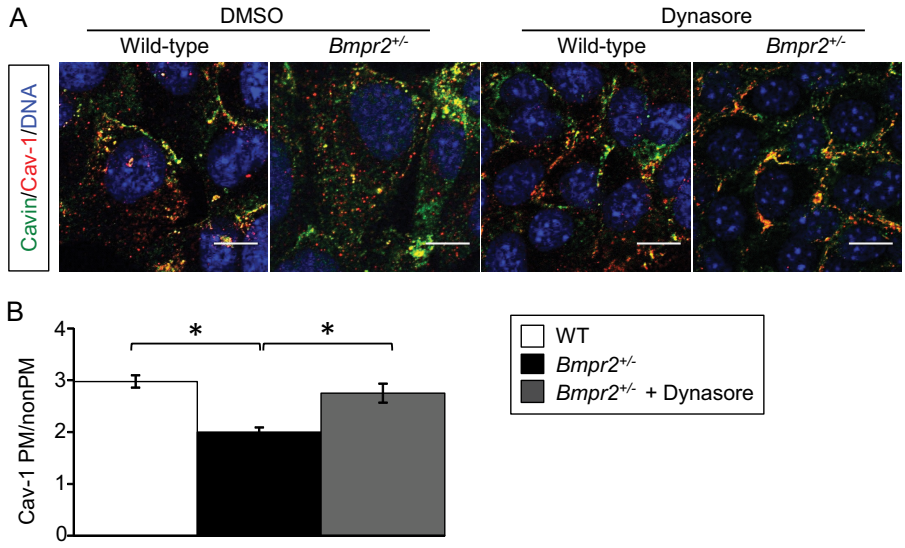

FIGURE 3. **Dynamin-2 inhibition restores CAV-1 localization to the plasma membrane in *Bmpr2*$^{+/-}$ PECs.** *A*, CAV-1 and Cavin-1 localization after dynasore treatment. Representative immunofluorescence images demonstrate CAV-1 and Cavin-1 localization following vehicle or 80 μM dynasore treatment for 30 min. *Scale bar*, 10 μm. *B*, quantitative analysis of CAV-1 localization after dynasore treatment. Values are expressed as the mean ratios of plasma membrane (*PM*) to non-plasma membrane fluorescence intensities in multiple cells from three wild-type lines ($n = 100$), three untreated *Bmpr2*$^{+/-}$ lines ($n = 100$), and two *Bmpr2*$^{+/-}$ lines after dynasore treatment ($n = 60$). *Error bars* represent S.E. *, $p < 0.001$ (one-way ANOVA with Dunnett's correction for repeated comparisons with untreated *Bmpr2*$^{+/-}$ PECs).

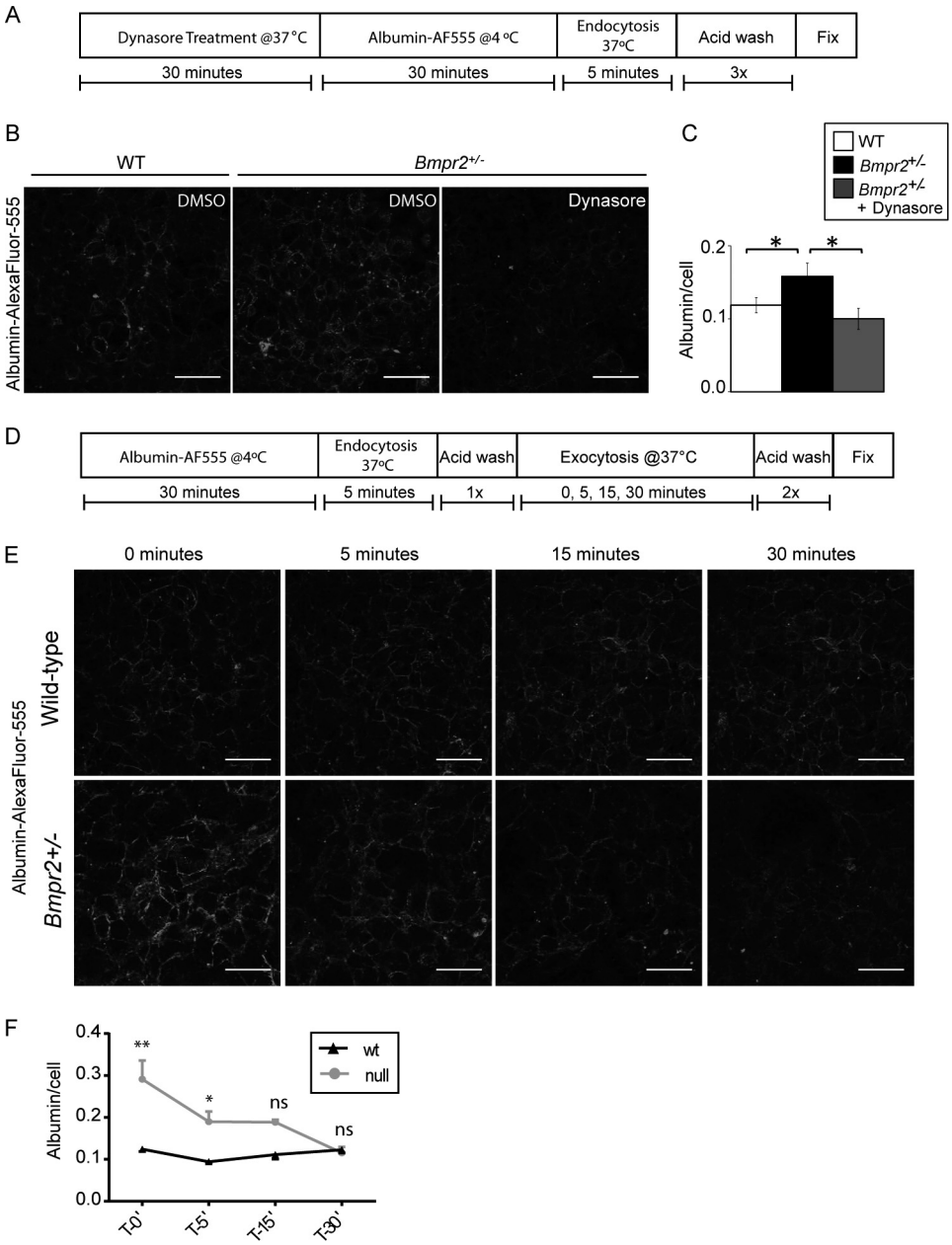

FIGURE 4. ***Bmpr2*$^{+/-}$ PECs have increased caveolar endocytosis but exhibit normal exocytosis.** *A*, schematic illustrating experimental setup in *B*. *B*, increased albumin uptake in *Bmpr2*$^{+/-}$ PECs is ablated in *Bmpr2*$^{+/-}$ PECs pretreated with dynasore. Representative immunofluorescence images demonstrate albumin localization following vehicle or 80 μM dynasore treatment for 30 min. Cells were incubated in 0.1 mg/ml albumin-Alexa Fluor (*AF*) 555 for 5 min at 37 °C in DMSO or dynasore as indicated followed by acid stripping to removed membrane-bound albumin as outlined in *A*. *Scale bars*, 50 μm. *C*, quantitative analysis of albumin uptake in *B*. Values are expressed as the mean fluorescence intensity divided by total cell number. *Error bars* represent S.E. *, $p < 0.05$ (one-way ANOVA with Dunnett's correction for multiple comparisons with untreated *Bmpr2*$^{+/-}$ PECs). *D*, schematic illustrating experimental setup in *E*. *E*, representative immunofluorescence images demonstrating albumin exocytosis following 5 min of endocytosis. Cells were incubated in 0.1 mg/ml albumin-Alexa Fluor 555 for 5 min at 37 °C followed by one round of acid stripping. Cells were then returned to 37 °C for the indicated times and subsequently fixed. *Scale bars*, 50 μm. *F*, quantitative analysis of albumin exocytosis in *E*. Values are expressed as the mean fluorescence intensity divided by total cell number. *Error bars* represent S.E. *, $p < 0.01$; **, $p < 0.0001$; *ns*, not significant (two-way repeated measures ANOVA with Šidák's correction for multiple comparisons with *Bmpr2*$^{+/-}$ PECs). ′, minutes.

Increased Caveolar Endocytosis in Bmpr2$^{+/-}$ *PECs*—To determine whether *Bmpr2*$^{+/-}$ PECs have increased endocytosis, we evaluated the uptake of fluorescently labeled albumin in wild-type and *Bmpr2*$^{+/-}$ PECs. Using the assay outlined in Fig. 4*A*, we show *Bmpr2*$^{+/-}$ PECs have increased uptake of albumin-Alexa Fluor 555 and that this is blocked in cells pretreated with dynasore (Fig. 4, *B* and *C*), suggesting *Bmpr2*$^{+/-}$ PECs have increased caveolar endocytosis. However, this assay does not rule out potential defects in exocytosis. To exclude this possibility, we evaluated exocytosis in wild-type and *Bmpr2*$^{+/-}$ PECs as outlined in Fig. 4*D*. We demonstrate that *Bmpr2*$^{+/-}$ PECs have no defect in exocytosis as intracellular albumin levels return to levels similar to wild type as early as 15 min following endocytosis of albumin (Fig. 4, *E* and *F*). These data demonstrate that *Bmpr2*$^{+/-}$ PECs have increased endocytosis contributing to mislocalization of CAV-1 and accumula-

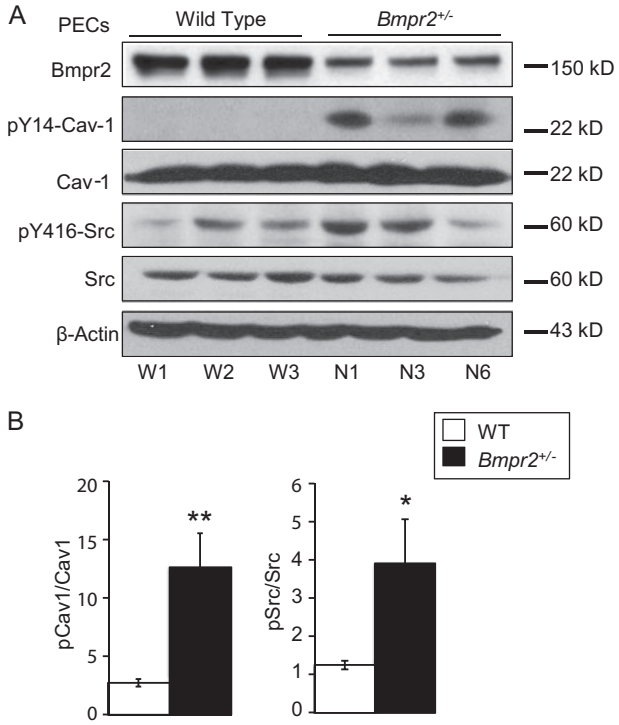

FIGURE 5. **Increased SRC and CAV-1 phosphorylation in *Bmpr2*$^{+/-}$ PECs.** *A*, Western blots demonstrating basal expression of phosphorylated Tyr^{14}-CAV-1 and Tyr^{416}-SRC and total BMPR2, CAV-1, and SRC kinase from three wild-type (W1, W2, and W3) and three *Bmpr2*$^{+/-}$ (N1, N3, and N6) PEC lines. β-Actin serves as a loading control. *B*, quantitative analysis of Western blot band densitometry values from four independent experimental replicates for a total of 12 samples per genotype. Values are expressed as the mean ratios of band densities as indicated. *Error bars* represent S.E. *, $p < 0.0001$; **, $p < 0.001$ *versus* wild-type controls (*t* test). Gels were run and probed as follows: Gel 1, BMPR2; Gel 2, Tyr(P)^{14}-CAV-1, Tyr(P)^{416}-SRC, and β-actin; Gel 3, CAV-1 and SRC. *pCav1*, phosphorylated CAV-1; *pSrc*, phosphorylated SRC.

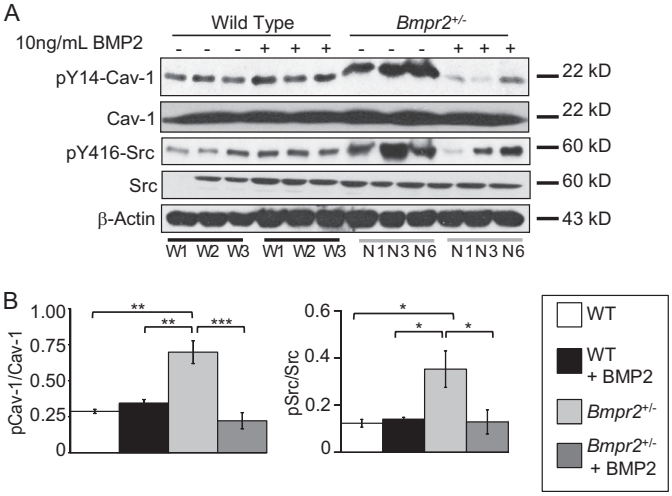

FIGURE 6. **BMP2 stimulation reduces SRC activity in *Bmpr2*$^{+/-}$ PECs.** *A*, Western blot analysis of Tyr(P)^{14}- and total CAV-1 and Tyr(P)^{416}- and total SRC following vehicle or 10 ng/ml BMP2 ligand treatment for 1 h in three wild-type (W1, W2, and W3) and three *Bmpr2*$^{+/-}$ (N1, N3, and N6) PEC lines. *B*, quantification of band densitometry in *A*. Values are expressed as the mean ratios of band densities as indicated. *Error bars* represent S.E. *, $p < 0.05$; **, $p < 0.01$; ***, $p < 0.001$ (one-way ANOVA with Dunnett's correction for comparisons with untreated *Bmpr2*$^{+/-}$ PECs). Gels were run and probed as follows: Gel 1, Tyr(P)^{14}-CAV-1, Tyr(P)^{416}-SRC, and β-actin; Gel 2, CAV-1 and SRC. *pCav-1*, phosphorylated CAV-1; *pSrc*, phosphorylated SRC.

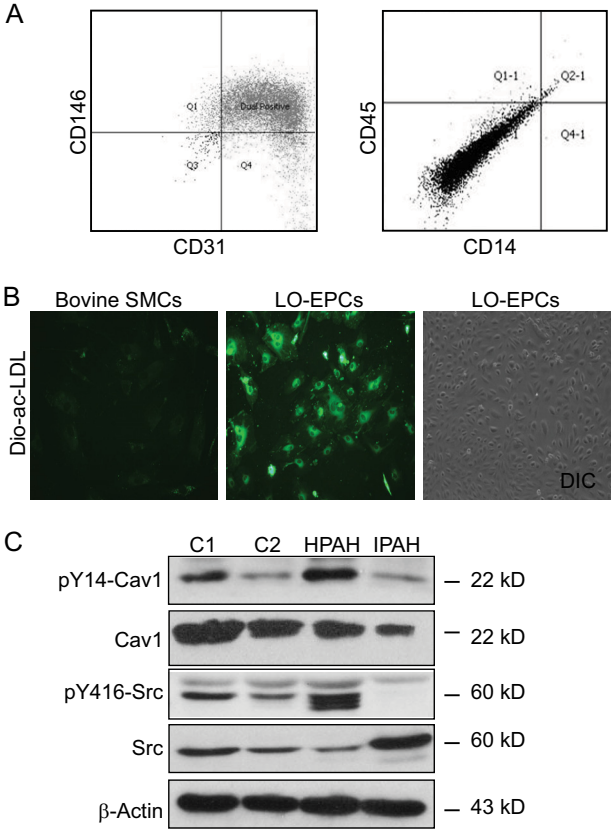

FIGURE 7. **Increased SRC activity in HPAH patient-derived LO-EPCs.** *A*, LO-EPCs express endothelial cell markers. Patient-derived LO-EPCs are positive for two endothelial cell markers, CD146 and CD31, and negative for leukocyte and macrophage markers CD45 and CD14 as analyzed by FACS. *B*, Dio-Ac-LDL uptake. LO-EPCs take up endothelium-specific Dio-Ac-LDL and exhibit cobblestone-like morphology. Bovine aortic smooth muscle cells (*SMCs*) serve as negative controls. *C*, increased SRC activity in HPAH patient-derived LO-PECs. A Western blot depicts basal protein expression of Tyr(P)^{14}- and total CAV-1 and Tyr(P)^{416}- and total SRC in LO-PECs from two disease-free controls (*C1* and *C2*), one HPAH patient (*BMPR2 V299 FsX1*), and one IPAH patient negative for *BMPR2* mutations. β-Actin serves as a loading control. Gels were run and probed as follows: Gel 1, Tyr(P)^{14}-CAV-1, Tyr(P)^{416}-SRC, and β-actin; Gel 2, CAV-1 and SRC. *DIC*, differential interference contrast.

tion of intracellular albumin but exhibit no defects in exocytosis.

Increased SRC Kinase Activity in Bmpr2$^{+/-}$ *PECs*—Dynamin-dependent caveolar endocytosis is initiated by the SRC-mediated phosphorylation of CAV-1 on Tyr^{14} (17, 38, 39). Western blot analysis indicates that there is increased phosphorylated (Tyr(P)^{14}) CAV-1 as well as increased expression of activated phosphorylated (Tyr(P)^{416}) SRC kinase in *Bmpr2*$^{+/-}$ PECs (Fig. 5, *A* and *B*).

Previous studies have shown that BMPR2 interacts with SRC and that BMPs reduce basal Tyr(P)^{416}-SRC expression in pulmonary artery smooth muscle cells (40). We were unable to detect interaction between SRC and BMPR2 in wild-type PECs after immunoprecipitation with SRC or Bmpr2 antibodies (data not shown). Moreover, BMP2 had no effect on basal Tyr(P)^{14}-CAV-1 or Tyr(P)^{416}-SRC expression in wild-type PECs (Fig. 6, *A* and *B*). However, treatment with BMP2 reduces Tyr(P)^{14}-CAV-1 and Tyr(P)^{416}-SRC expression in *Bmpr2*$^{+/-}$ PECs, indicating that BMP2 reverses aberrant SRC-dependent CAV-1 phosphorylation in *Bmpr2*$^{+/-}$ PECs. Because treatment with

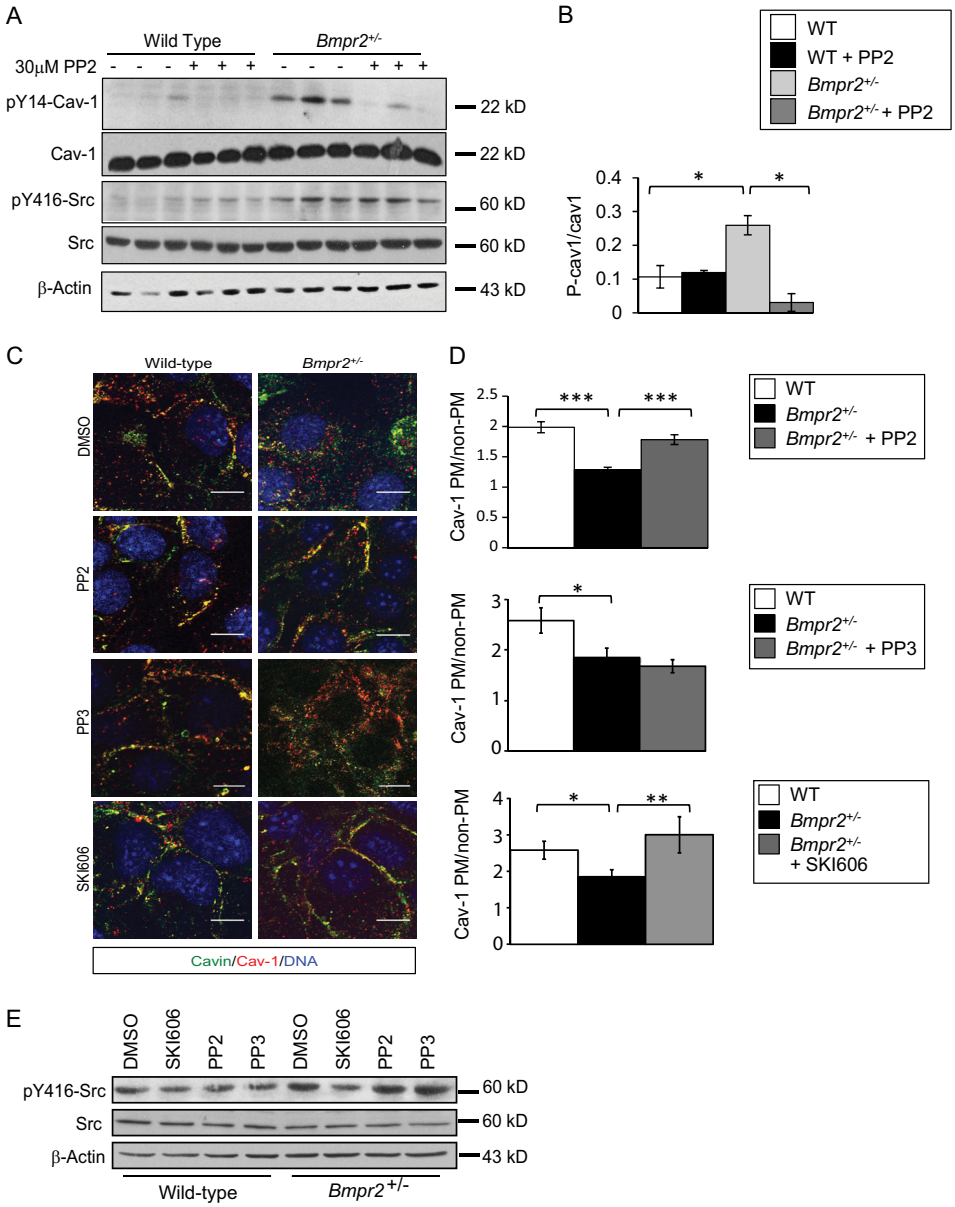

FIGURE 8. **SRC inhibition with PP2 reduces Tyr(P)^{14}-CAV-1 and restores CAV-1 localization to the plasma membrane in *Bmpr2*$^{+/-}$ PECs.** *A*, PP2 inhibits Tyr^{14}-CAV-1 phosphorylation. Cells were treated with 30 μM PP2 for 30 min prior to cell lysis. The experiment was performed in triplicate in one wild-type line (W1) and one *Bmpr2*$^{+/-}$ line (N1). SRC inhibition is demonstrated by reduced phosphorylation of the SRC target Tyr(P)^{14}-CAV-1. *B*, quantification of band densitometry in *A*. Values are expressed as the mean ratios of band densities as indicated. *Error bars* represent S.E. *, $p < 0.01$ *versus* wild-type controls (*t* test). *P-cav1*, phosphorylated CAV-1. *C*, CAV-1 and Cavin-1 localization after PP2, PP3, or SKI606 treatment. Representative immunofluorescence images show CAV-1 and Cavin-1 localization after treatment. *Scale bars*, 10 μm. *D*, quantitative analysis of CAV-1 localization after treatment. Values are expressed as the mean ratio of plasma membrane (*PM*) to non-plasma membrane fluorescence intensities in multiple cells from one wild-type (W1; $n = 45$) and one *Bmpr2*$^{+/-}$ line (N1; $n = 75$) before and after PP2 treatment (W1, $n = 33$; N1, $n = 35$; N1 PP3, $n = 10$; N1 SKI606, $n = 14$). *Error bars* represent S.E. *, $p < 0.05$; **, $p < 0.01$; ***, $p < 0.0001$ (one-way ANOVA with Dunnett's and the Holm-Šidák correction for comparisons with untreated *Bmpr2*$^{+/-}$ PECs, respectively). *E*, SKI606 inhibits SRC phosphorylation at Tyr^{416}. Cells were treated with 30 μM PP2, 30 μM PP3, or 1 μM SKI606 for 30 min prior to cell lysis. Gels were run and probed as follows: *A*, Gel 1, Tyr(P)^{14}-CAV-1, Tyr(P)^{416}-SRC, and β-actin; Gel 2, CAV-1 and SRC; *E*, Gel 1, Tyr(P)^{416}-SRC; Gel 2, SRC and β-actin.

BMP ligands activates basal BMPR2 signaling, these data suggest that defective BMPR2 signaling promotes constitutive SRC activation in *Bmpr2*$^{+/-}$ PECs.

Increased SRC Activation in HPAH Patient LO-EPCs—To determine whether SRC activation also occurs in endothelial cells from HPAH patients carrying germ line heterozygous null mutations at the *BMPR2* locus, we isolated LO-EPCs from an HPAH patient with a known *BMPR2* mutation (Family 164, *BMPR2 V299 FsX1* (*BMPR2 893 ins GG*)) and an IPAH patient without a known *BMPR2* mutation. As described previously (41), LO-EPCs are rapidly proliferating cells with endothelial morphology that express endothelial cell markers CD31 and CD146 and take up Dio-Ac-LDL but unlike early outgrowth EPCs do not express markers of the macrophage lineage (Fig. 7, *A* and *B*). They therefore provide a readily accessible, renewable source of endothelial cells from patients with this rare genetic disorder. Using these cells, we show that there is an increase in Tyr(P)^{416}-SRC and Tyr(P)^{14}-CAV-1 expression in the HPAH patient-derived LO-EPCs compared with two normal controls and the IPAH patient-derived cells (Fig. 7*C*), suggesting that

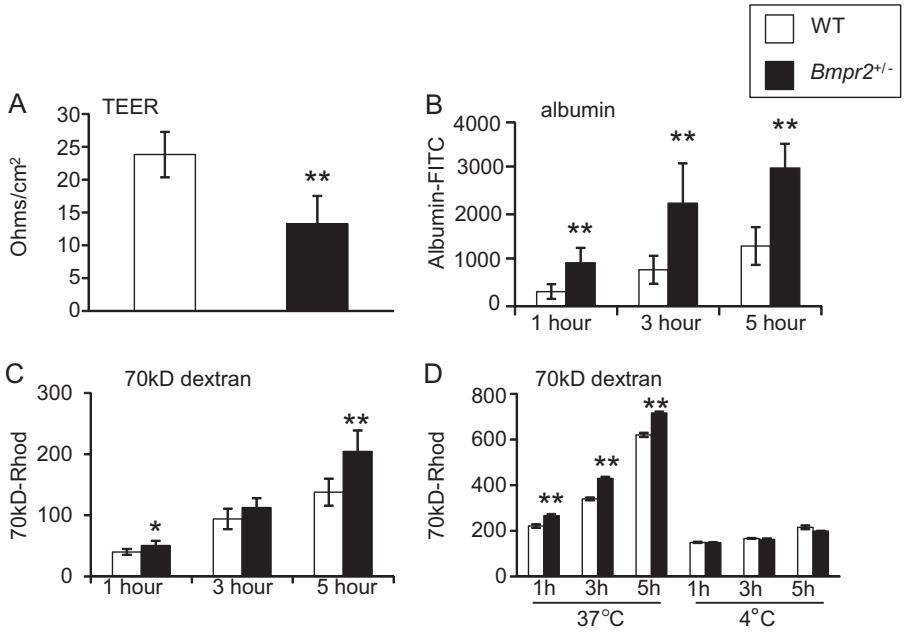

FIGURE 9. **Impaired endothelial barrier function in *Bmrp2*$^{+/-}$ PECs.** *A*, TEER in three wild-type and three *Bmpr2*$^{+/-}$ PEC lines. *B* and *C*, transwell permeability assays for FITC-albumin (*B*) and rhodamine-70-kDa dextran (*70kD-Rhod*). (*C*). Studies were performed in triplicate in three wild-type lines and three *Bmpr2*$^{+/-}$ lines. *D*, comparison of permeability to rhodamine-70-kDa dextran at 37 and 4 °C. Transwell permeability assays were performed in wild-type (W1) and *Bmpr2*$^{+/-}$ (N6) PECs with six replicates/genotype/condition. All results are expressed as the mean. *Error bars* represent S.E. *, $p < 0.01$; **, $p < 0.001$ *versus* wild-type controls (*t* test).

defects in SRC kinase and CAV-1 may be applicable to human disease.

SRC Inhibition Restores CAV-1 Localization to the Plasma membrane in Bmpr2$^{+/-}$ *PECs*—To determine whether increased intracellular localization of CAV-1 results from constitutive activation of SRC in *Bmpr2*$^{+/-}$ PECs, we first determined whether inhibition of SRC kinase activity reduces basal Tyr^{14}-CAV-1 phosphorylation in *Bmpr2*$^{+/-}$ PECs. Treatment with the selective SRC family kinase inhibitor PP2 (42) decreases CAV-1 Tyr^{14} phosphorylation in *Bmpr2*$^{+/-}$ PECs (Fig. 8, *A* and *B*). These findings indicate that increased SRC kinase activity causes the increase in basal CAV-1 phosphorylation in *Bmpr2*$^{+/-}$ PECs. Because SRC-dependent phosphorylation of Tyr^{14}-CAV-1 promotes caveolar endocytosis (17, 38, 39), we sought to determine whether constitutive activation of SRC kinase also increases intracellular localization of CAV-1 in *Bmpr2*$^{+/-}$ PECs. Treatment with PP2 restores plasma membrane localization of CAV-1 in *Bmpr2*$^{+/-}$ PECs (Fig. 8, *E* and *F*), suggesting that caveolar defects result from increased SRC-dependent caveolar endocytosis in *Bmpr2*$^{+/-}$ PECs. To confirm that these effects were due to inhibition of SRC kinase and not off-target effects, we used an additional SRC kinase inhibitor, SKI606 (43), and a PP2 analog with no activity, PP3. We show SKI606 reduces SRC phosphorylation at Tyr^{416} in *Bmpr2*$^{+/-}$ PECs, whereas PP3 has no effect (Fig. 8, *C* and *D*). Furthermore, we show that SKI606 is able to rescue CAV-1 localization to the plasma membrane in *Bmpr2*$^{+/-}$ PECs, similar to PP2, whereas PP3 had no effects on CAV-1 localization (Fig. 8, *E* and *F*), demonstrating that restoration of CAV-1 to the plasma membrane is due to inhibition of SRC kinase activity.

Impaired Endothelial Barrier Function in Bmpr2$^{+/-}$ *PECs*—Because enhanced caveolar endocytosis promotes increased endothelial cell permeability (18, 19), we determined whether *Bmpr2*$^{+/-}$ PEC monolayers have decreased barrier function. There is a significant reduction in TEER across confluent monolayers of *Bmpr2*$^{+/-}$ PECs compared with wild-type controls (Fig. 9*A*), indicating endothelial barrier dysfunction. To determine whether impaired endothelial barrier function in *Bmpr2*$^{+/-}$ PECs is associated with enhanced transcellular permeability, we used Transwell assays to assess permeability to two high molecular weight solutes that are transported through the endothelium by caveolar endocytosis, albumin and 70-kDa dextran (44). *Bmpr2*$^{+/-}$ PECs have increased permeability to both albumin and 70-kDa dextran compared with wild-type PECs (Fig. 9, *B* and *C*). Taken together, these data suggest that there is a defect in paracellular and transcellular barrier function in *Bmpr2*$^{+/-}$ PECs. To determine whether increased endothelial permeability to high molecular weight solutes results from differences in active endocytic trafficking rather than a paracellular defect in permeability, we repeated this assay in cells cultured at 4 °C because endocytosis is a temperature-sensitive process that is completely blocked at 4 °C (31–33). As anticipated, when cultured at 4 °C, wild-type and *Bmpr2*$^{+/-}$ PECs exhibit reduced permeability to 70-kDa dextran, but there is no discernible difference between genotypes (Fig. 9*D*). Similar effects were seen with FITC-albumin (data not shown). These data indicate that enhanced permeability to high molecular weight solutes results from enhanced endocytic transcellular and not paracellular transport in *Bmpr2*$^{+/-}$ PECs.

SRC Inhibition Partially Restores Endothelial Barrier Function in Bmpr2$^{+/-}$ *PECs*—To determine whether defective endothelial barrier function is due to increased SRC activity, we assessed whether SRC inhibition would ameliorate endothelial barrier dysfunction in *Bmpr2*$^{+/-}$ PECs. TEER and permeability to 70-kDa dextran in *Bmpr2*$^{+/-}$ PECs is restored to wild-type levels following SRC inhibition with PP2 (Fig. 10, *A* and *B*).

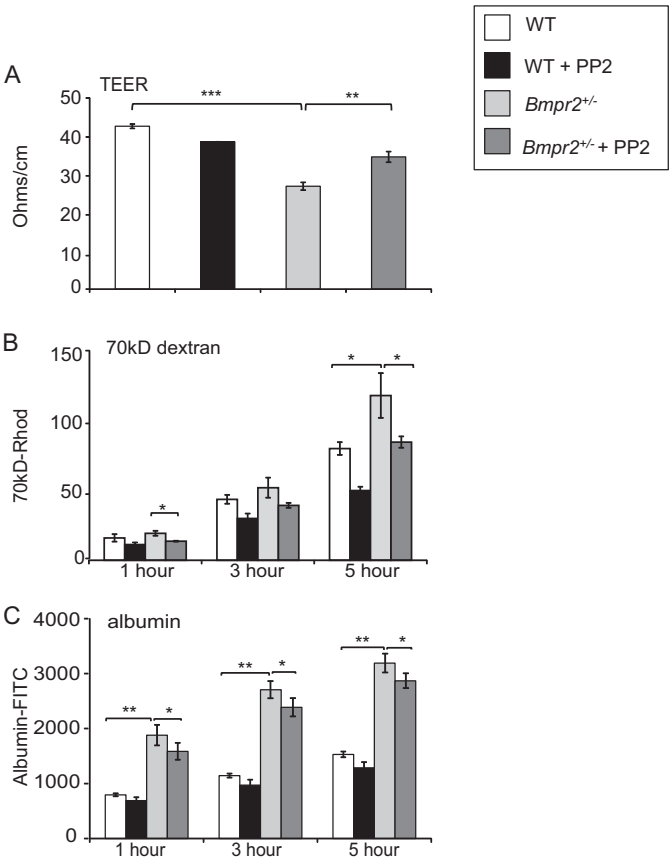

FIGURE 10. **SRC inhibition with PP2 improves endothelial barrier function in *Bmrp2*$^{+/-}$ PECs.** *A*, TEER. TEER was evaluated 30 min after treatment with 30 μM PP2. *B* and *C*, Transwell permeability for rhodamine-70-kDa dextran (*70kD-Rhod*) (*B*) and FITC-albumin (*C*). Cells were treated with 30 μM PP2 for 30 min before adding fluorophore-conjugated solutes. Studies were performed in wild-type (W1) and *Bmpr2*$^{+/-}$ PECs (N6) in triplicate. Results are expressed as the mean. *Error bars* represent S.E. *, $p < 0.05$; **, $p < 0.01$; ***, $p < 0.001$ *versus* untreated *Bmpr2*$^{+/-}$ PECs (*t* test).

There is also a reduction in permeability to albumin after treatment with PP2, but these levels do not return to those of wild-type PECs (Fig. 10*C*). These data indicate that *Bmpr2*$^{+/-}$ PECs have impaired barrier function due in part to constitutive activation of SRC kinase. Because SRC inhibition restores the caveolar trafficking in *Bmpr2*$^{+/-}$ PECs, our findings also suggest that abnormal SRC-mediated caveolar trafficking plays a role in promoting decreased barrier function in *Bmpr2*$^{+/-}$ PECs.

DISCUSSION

Several studies implicate altered caveolae and CAV-1 in endothelial dysfunction and the pathogenesis of pulmonary hypertension (21, 23–25, 45), but to date, the link between caveolar dysfunction and *BMPR2* mutations in HPAH has not been established. In these studies, we have used PECs from *Bmpr2*$^{+/-}$ mice to show that a heterozygous null *Bmpr2* mutation gives rise to increased numbers of internalized caveolae and core caveolar structural proteins CAV-1 and Cavin-1 in the pulmonary endothelium. We have also shown that aberrant intracellular localization of CAV-1 in *Bmpr2*$^{+/-}$ PECs is restored to the plasma membrane after treatment with either a Dynamin-2 or SRC kinase inhibitor. This suggests that increased numbers of caveolae in *Bmpr2*$^{+/-}$ PECs result from increased dynamin-dependent caveolar endocytosis and that this defect is the result of constitutive activation of SRC kinase that we also observed in *Bmpr2*$^{+/-}$ PECs. We have also shown increased SRC activity in LO-EPCs isolated from HPAH patients. These findings are consistent with previous studies showing increased numbers of caveolae and increased SRC activity in the lungs of patients with idiopathic PAH (46, 47) and suggest a mechanism by which *BMPR2* mutations give rise to endothelial dysfunction in HPAH.

There is evidence that endothelial barrier dysfunction and perivascular inflammation contribute to pathogenesis of PAH (14–16). Our findings that PECs from *Bmpr2*$^{+/-}$ mice have decreased barrier function are also consistent with data showing that mice with conditional *Bmpr2* deletion in the endothelium develop spontaneous pulmonary hypertension and have increased vascular leak and perivascular inflammation (11–13). However, the mechanism by which *Bmpr2* deficiency decreases endothelial barrier function was unknown. Caveolae regulate endothelial cell permeability by promoting endocytic transcellular transport of macromolecules (18–20) and to a lesser extent by recycling components of the endothelial tight junctions to increase paracellular transport (48, 49). Our data show that both paracellular and transcellular barrier function is impaired in *Bmpr2*$^{+/-}$ PECs. Although there is cross-talk between transcellular and paracellular permeability pathways in endothelial cells (50), we also have shown that increased permeability to the high molecular weight solutes is diminished by culturing *Bmpr2*$^{+/-}$ PECs at 4 °C, indicating that *Bmpr2*$^{+/-}$ PECs have a defect in endocytic transcellular permeability. However, SRC kinase also increases paracellular permeability in endothelial cells by promoting cytoskeletal contraction and by inducing dissociation of junctional complexes (51), so it is possible that some of the effects of the SRC family kinase inhibitor PP2 on paracellular permeability in *Bmpr2*$^{+/-}$ PECs are mediated through non-caveolar mechanisms.

We also have shown that there is increased intracellular accumulation of another core caveolar structural protein, Cavin-1, and that there are increased numbers of intracellular caveolar structures in the pulmonary endothelium of *Bmpr2*$^{+/-}$ mice. These findings suggest that mislocalization of CAV-1 results from abnormalities in caveolae rather than mistrafficking of individual protein monomers in *Bmpr2*$^{+/-}$ PECs. In addition, we have shown that blocking phosphorylation of Tyr^{14}-CAV-1 with PP2 restores CAV-1 localization to the plasma membrane in *Bmpr2*$^{+/-}$ PECs, suggesting that intracellular accumulation of endogenously expressed CAV-1 in *Bmpr2*$^{+/-}$ PEC is dependent on SRC-mediated Tyr(P)^{14}-CAV-1 phosphorylation. This effect is distinct from the intracellular accumulation of CAV-1 that occurs when CAV-1 levels are increased as has been shown to occur without Tyr^{14}-CAV-1 phosphorylation (52).

The mechanism by which heterozygous loss of BMPR2 expression in *Bmpr2*$^{+/-}$ PECs promotes constitutive activation of SRC kinase remains to be established. However, there is evidence that SRC kinase is activated in the lungs of patients with idiopathic PAH (46, 47). Furthermore, published data suggest that the C terminus of BMPR2 binds to and inhibits SRC kinase activity and that BMP stimulation reduces SRC activity in pul-

monary artery smooth muscle cells (40). We were unable to reproduce these findings in wild-type PECs. This discrepancy is likely to reflect transient and weak interactions between SRC and BMPR2 and/or differences in molecular behavior of these proteins in two distinct cell types. However, we did observe a marked reduction on Tyr(P)^{416}-SRC and Tyr(P)^{14}-CAV-1 in *Bmpr2*$^{+/-}$ PECs after treatment with BMP2, suggesting that restoration of BMP signaling in these cells is sufficient to reverse these effects. These findings have therapeutic implications because they suggest that activation of the BMP signaling pathway with BMP agonists, either secreted ligands or small molecule activators such as THR-123 or FK506 (53, 54), might be used to reverse SRC-dependent endothelial dysfunction in HPAH patients with *BMPR2* mutations.

Therapeutic strategies targeted toward restoring endothelial barrier integrity may be beneficial for the treatment of patients with PAH. Here we have shown that SRC kinase inhibition with the pharmacological inhibitor PP2 improves endothelial barrier function in *Bmpr2*$^{+/-}$ PECs, suggesting that the constitutive activation of SRC kinase in pulmonary endothelium of HPAH patients carrying heterozygous *BMPR2* mutations may provide an attractive therapeutic target for this disease. SRC activation has also been identified in patients with idiopathic PAH (46, 47), suggesting that therapeutic inhibition of SRC activity may be applicable to a wider range of patients with this disease. Furthermore, because SRC-dependent caveolar dysfunction may also promote endothelial dysfunction through deregulation of endothelial NOS activity (17, 37), this strategy may have more extensive beneficial effects on pulmonary vascular disease pathophysiology in patients with HPAH.

Acknowledgments—We thank the Vanderbilt University EM core for help preparing and analyzing transmission EM samples, the Vanderbilt University Shared Resources Imaging Core for help imaging confocal immunofluorescence samples, the Veterans Affairs flow cytometry core for FACS analysis, and H. Beppu for the generous gift of Bmpr2$^{+/-}$ *mice. We wish to thank Dr. Matthew Tyska and Dr. James Goldenring for their advice on confocal imaging and trafficking assays, respectively.*

REFERENCES

1. Humbert, M., Sitbon, O., Chaouat, A., Bertocchi, M., Habib, G., Gressin, V., Yaïci, A., Weitzenblum, E., Cordier, J. F., Chabot, F., Dromer, C., Pison, C., Reynaud-Gaubert, M., Haloun, A., Laurent, M., Hachulla, E., Cottin, V., Degano, B., Jaïs, X., Montani, D., Souza, R., and Simonneau, G. (2010) Survival in patients with idiopathic, familial, and anorexigen-associated pulmonary arterial hypertension in the modern management era. *Circulation* **122,** 156–163
2. International PPH Consortium, Lane, K. B., Machado, R. D., Pauciulo, M. W., Thomson, J. R., Phillips, J. A., 3rd, Loyd, J. E., Nichols, W. C., and Trembath, R. C. (2000) Heterozygous germline mutations in BMPR2, encoding a TGF-β receptor, cause familial primary pulmonary hypertension. *Nat. Genet.* **26,** 81–84
3. Loyd, J. E., and Phillips, J. A., III (2012) in *GeneReviews®* (Pagon, R. A., Adam, M. P., Bird, T. D., Dolan, C. R., Fong, C.-T., Smith, R. J. H., and Stephens, K., eds) www.ncbi.nlm.nih.gov/books/NBK1485/, University of Seattle, Seattle, WA
4. Atkinson, C., Stewart, S., Upton, P. D., Machado, R., Thomson, J. R., Trembath, R. C., and Morrell, N. W. (2002) Primary pulmonary hypertension is associated with reduced pulmonary vascular expression of type II bone morphogenetic protein receptor. *Circulation* **105,** 1672–1678
5. Morrell, N. W., Yang, X., Upton, P. D., Jourdan, K. B., Morgan, N., Sheares, K. K., and Trembath, R. C. (2001) Altered growth responses of pulmonary artery smooth muscle cells from patients with primary pulmonary hypertension to transforming growth factor-1 and bone morphogenetic proteins. *Circulation* **104,** 790–795
6. Richter, A., Yeager, M. E., Zaiman, A., Cool, C. D., Voelkel, N. F., and Tuder, R. M. (2004) Impaired transforming growth factor β signaling in idiopathic pulmonary arterial hypertension. *Am. J. Respir. Crit. Care Med.* **170,** 1340–1348
7. Lowery, J. W., and de Caestecker, M. P. (2010) BMP signaling in vascular development and disease. *Cytokine Growth Factor Rev.* **21,** 287–298
8. Frank, D. B., Lowery, J., Anderson, L., Brink, M., Reese, J., and de Caestecker, M. (2008) Increased susceptibility to hypoxic pulmonary hypertension in Bmpr2 mutant mice is associated with endothelial dysfunction in the pulmonary vasculature. *Am. J. Physiol. Lung Cell. Mol. Physiol.* **294,** L98–L109
9. Ramos, M., Lamé, M. W., Segall, H. J., and Wilson, D. W. (2006) The BMP type II receptor is located in lipid rafts, including caveolae, of pulmonary endothelium *in vivo* and *in vitro*. *Vascul. Pharmacol.* **44,** 50–59
10. Takahashi, H., Goto, N., Kojima, Y., Tsuda, Y., Morio, Y., Muramatsu, M., and Fukuchi, Y. (2006) Downregulation of type II bone morphogenic protein receptor in hypoxic pulmonary hypertension. *Am. J. Physiol. Lung Cell. Mol. Physiol.* **290,** L450–L458
11. Burton, V. J., Ciuclan, L. I., Holmes, A. M., Rodman, D. M., Walker, C., and Budd, D. C. (2011) Bone morphogenetic protein receptor II regulates pulmonary artery endothelial cell barrier function. *Blood* **117,** 333–341
12. Burton, V. J., Holmes, A. M., Ciuclan, L. I., Robinson, A., Roger, J. S., Jarai, G., Pearce, A. C., and Budd, D. C. (2011) Attenuation of leukocyte recruitment via CXCR1/2 inhibition stops the progression of PAH in mice with genetic ablation of endothelial BMPR-II. *Blood* **118,** 4750–4758
13. Hong, K. H., Lee, Y. J., Lee, E., Park, S. O., Han, C., Beppu, H., Li, E., Raizada, M. K., Bloch, K. D., and Oh, S. P. (2008) Genetic ablation of the BMPR2 gene in pulmonary endothelium is sufficient to predispose to pulmonary arterial hypertension. *Circulation* **118,** 722–730
14. Savai, R., Pullamsetti, S. S., Kolbe, J., Bieniek, E., Voswinckel, R., Fink, L., Scheed, A., Ritter, C., Dahal, B. K., Vater, A., Klussmann, S., Ghofrani, H. A., Weissmann, N., Klepetko, W., Banat, G. A., Seeger, W., Grimminger, F., and Schermuly, R. T. (2012) Immune/inflammatory cell involvement in the pathology of idiopathic pulmonary arterial hypertension. *Am. J. Respir. Crit. Care Med.* **186,** 897–908
15. Stacher, E., Graham, B. B., Hunt, J. M., Gandjeva, A., Groshong, S. D., McLaughlin, V. V., Jessup, M., Grizzle, W. E., Aldred, M. A., Cool, C. D., and Tuder, R. M. (2012) Modern age pathology of pulmonary arterial hypertension. *Am. J. Respir. Crit. Care Med.* **186,** 261–272
16. Dorfmüller, P., Perros, F., Balabanian, K., and Humbert, M. (2003) Inflammation in pulmonary arterial hypertension. *Eur. Respir. J.* **22,** 358–363
17. Parat, M.-O. (2009) The biology of caveolae: achievements and perspectives. *Int. Rev. Cell Mol. Biol.* **273,** 117–162
18. Sun, Y., Minshall, R. D., and Hu, G. (2011) Role of caveolin-1 in the regulation of pulmonary endothelial permeability. *Methods Mol. Biol.* **763,** 303–317
19. Minshall, R. D., Sessa, W. C., Stan, R. V., Anderson, R. G., and Malik, A. B. (2003) Caveolin regulation of endothelial function. *Am. J. Physiol. Lung Cell. Mol. Physiol.* **285,** L1179–L1183
20. Sowa, G. (2012) Caveolae, caveolins, cavins, and endothelial cell function: new insights. *Front. Physiol.* **2,** 120
21. Maniatis, N. A., Shinin, V., Schraufnagel, D. E., Okada, S., Vogel, S. M., Malik, A. B., and Minshall, R. D. (2008) Increased pulmonary vascular resistance and defective pulmonary artery filling in caveolin-1−/− mice. *Am. J. Physiol. Lung Cell. Mol. Physiol.* **294,** L865–L873
22. Zhao, Y. Y., Zhao, Y. D., Mirza, M. K., Huang, J. H., Potula, H. H., Vogel, S. M., Brovkovych, V., Yuan, J. X., Wharton, J., and Malik, A. B. (2009) Persistent eNOS activation secondary to caveolin-1 deficiency induces pulmonary hypertension in mice and humans through PKG nitration. *J. Clin. Investig.* **119,** 2009–2018
23. Patel, H. H., Zhang, S., Murray, F., Suda, R. Y., Head, B. P., Yokoyama, U., Swaney, J. S., Niesman, I. R., Schermuly, R. T., Pullamsetti, S. S., Thistleth-

waite, P. A., Miyanohara, A., Farquhar, M. G., Yuan, J. X., and Insel, P. A. (2007) Increased smooth muscle cell expression of caveolin-1 and caveolae contribute to the pathophysiology of idiopathic pulmonary arterial hypertension. *FASEB J.* **21,** 2970–2979
24. Austin, E. D., Ma, L., LeDuc, C., Berman Rosenzweig, E., Borczuk, A., Phillips, J. A., 3rd, Palomero, T., Sumazin, P., Kim, H. R., Talati, M. H., West, J., Loyd, J. E., and Chung, W. K. (2012) Whole exome sequencing to identify a novel gene (caveolin-1) associated with human pulmonary arterial hypertension. *Circ. Cardiovasc. Genet.* **5,** 336–343
25. Asosingh, K., Farha, S., Lichtin, A., Graham, B., George, D., Aldred, M., Hazen, S. L., Loyd, J., Tuder, R., and Erzurum, S. C. (2012) Pulmonary vascular disease in mice xenografted with human BM progenitors from patients with pulmonary arterial hypertension. *Blood* **120,** 1218–1227
26. Beppu, H., Lei, H., Bloch, K. D., and Li, E. (2005) Generation of a floxed allele of the mouse BMP type II receptor gene. *Genesis* **41,** 133–137
27. Beppu, H., Kawabata, M., Hamamoto, T., Chytil, A., Minowa, O., Noda, T., and Miyazono, K. (2000) BMP type II receptor is required for gastrulation and early development of mouse embryos. *Dev. Biol.* **221,** 249–258
28. Anderson, L., Lowery, J. W., Frank, D. B., Novitskaya, T., Jones, M., Mortlock, D. P., Chandler, R. L., and de Caestecker, M. P. (2010) Bmp2 and Bmp4 exert opposing effects in hypoxic pulmonary hypertension. *Am. J. Physiol. Regul. Integr. Comp. Physiol.* **298,** R833–R842
29. Frank, D. B., Abtahi, A., Yamaguchi, D. J., Manning, S., Shyr, Y., Pozzi, A., Baldwin, H. S., Johnson, J. E., and de Caestecker, M. P. (2005) Bone morphogenetic protein 4 promotes pulmonary vascular remodeling in hypoxic pulmonary hypertension. *Circ. Res.* **97,** 496–504
30. Mead, L. E., Prater, D., Yoder, M. C., and Ingram, D. A. (2008) Isolation and characterization of endothelial progenitor cells from human blood. *Curr. Protoc. Stem Cell Biol.* **Chapter 2,** Unit 2C.1
31. Brickman, M. J., Cook, J. M., and Balber, A. E. (1995) Low temperature reversibly inhibits transport from tubular endosomes to a perinuclear, acidic compartment in African trypanosomes. *J. Cell Sci.* **108,** 3611–3621
32. Silverstein, S. C., Steinman, R. M., and Cohn, Z. A. (1977) Endocytosis. *Annu. Rev. Biochem.* **46,** 669–722
33. Rode, M., Berg, T., and Gjøen, T. (1997) Effect of temperature on endocytosis and intracellular transport in the cell line SHK-1 derived from salmon head kidney. *Comp. Biochem. Physiol. A Physiol.* **117,** 531–537
34. Henley, J. R., Krueger, E. W., Oswald, B. J., and McNiven, M. A. (1998) Dynamin-mediated internalization of caveolae. *J. Cell Biol.* **141,** 85–99
35. Macia, E., Ehrlich, M., Massol, R., Boucrot, E., Brunner, C., and Kirchhausen, T. (2006) Dynasore, a cell-permeable inhibitor of dynamin. *Dev. Cell* **10,** 839–850
36. Kirchhausen, T., Macia, E., and Pelish, H. E. (2008) Use of dynasore, the small molecule inhibitor of dynamin, in the regulation of endocytosis. *Methods Enzymol.* **438,** 77–93
37. Sbaa, E., Frérart, F., and Feron, O. (2005) The double regulation of endothelial nitric oxide synthase by caveolae and caveolin: a paradox solved through the study of angiogenesis. *Trends Cardiovasc. Med.* **15,** 157–162
38. Shajahan, A. N., Timblin, B. K., Sandoval, R., Tiruppathi, C., Malik, A. B., and Minshall, R. D. (2004) Role of Src-induced dynamin-2 phosphorylation in caveolae-mediated endocytosis in endothelial cells. *J. Biol. Chem.* **279,** 20392–20400
39. Hu, G., and Minshall, R. D. (2009) Regulation of transendothelial permeability by Src kinase. *Microvasc. Res.* **77,** 21–25
40. Wong, W. K., Knowles, J. A., and Morse, J. H. (2005) Bone morphogenetic protein receptor type II C-terminus interacts with c-Src: implication for a role in pulmonary arterial hypertension. *Am. J. Respir. Cell Mol. Biol.* **33,** 438–446
41. Reinisch, A., Hofmann, N. A., Obenauf, A. C., Kashofer, K., Rohde, E., Schallmoser, K., Flicker, K., Lanzer, G., Linkesch, W., Speicher, M. R., and Strunk, D. (2009) Humanized large-scale expanded endothelial colony-forming cells function *in vitro* and *in vivo*. *Blood* **113,** 6716–6725
42. Hanke, J. H., Gardner, J. P., Dow, R. L., Changelian, P. S., Brissette, W. H., Weringer, E. J., Pollok, B. A., and Connelly, P. A. (1996) Discovery of a novel, potent, and Src family-selective tyrosine kinase inhibitor: study of Lck- and Fyn-T-dependent cell activation. *J. Biol. Chem.* **271,** 695–701
43. Vultur, A., Buettner, R., Kowolik, C., Liang, W., Smith, D., Boschelli, F., and Jove, R. (2008) SKI-606 (bosutinib), a novel Src kinase inhibitor, suppresses migration and invasion of human breast cancer cells. *Mol. Cancer Ther.* **7,** 1185–1194
44. Minshall, R. D., Tiruppathi, C., Vogel, S. M., and Malik, A. B. (2002) Vesicle formation and trafficking in endothelial cells and regulation of endothelial barrier function. *Histochem. Cell Biol.* **117,** 105–112
45. Mathew, R., Huang, J., Shah, M., Patel, K., Gewitz, M., and Sehgal, P. B. (2004) Disruption of endothelial-cell caveolin-1alpha/raft scaffolding during development of monocrotaline-induced pulmonary hypertension. *Circulation* **110,** 1499–1506
46. Courboulin, A., Paulin, R., Giguère, N. J., Saksouk, N., Perreault, T., Meloche, J., Paquet, E. R., Biardel, S., Provencher, S., Côté, J., Simard, M. J., and Bonnet, S. (2011) Role for miR-204 in human pulmonary arterial hypertension. *J. Exp. Med.* **208,** 535–548
47. Paulin, R., Meloche, J., Jacob, M. H., Bisserier, M., Courboulin, A., and Bonnet, S. (2011) DHEA inhibits the Src/STAT3 constitutive activation in pulmonary arterial hypertension. *Am. J. Physiol. Heart Circ. Physiol.* **301,** H1798–H1809
48. Shen, L., and Turner, J. R. (2005) Actin depolymerization disrupts tight junctions via caveolae-mediated endocytosis. *Mol. Biol. Cell* **16,** 3919–3936
49. Stamatovic, S. M., Keep, R. F., Wang, M. M., Jankovic, I., and Andjelkovic, A. V. (2009) Caveolae-mediated internalization of occludin and claudin-5 during CCL2-induced tight junction remodeling in brain endothelial cells. *J. Biol. Chem.* **284,** 19053–19066
50. Van Driessche, W., Kreindler, J. L., Malik, A. B., Margulies, S., Lewis, S. A., and Kim, K.-J. (2007) Interrelations/cross talk between transcellular transport function and paracellular tight junctional properties in lung epithelial and endothelial barriers. *Am. J. Physiol. Lung Cell. Mol. Physiol.* **293,** L520–L524
51. Kim, L. C., Song, L., and Haura, E. B. (2009) Src kinases as therapeutic targets for cancer. *Nat. Rev. Clin. Oncol.* **6,** 587–595
52. Hanson, C. A., Drake, K. R., Baird, M. A., Han, B., Kraft, L. J., Davidson, M. W., and Kenworthy, A. K. (2013) Overexpression of caveolin-1 is sufficient to phenocopy the behavior of a disease-associated mutant. *Traffic* **14,** 663–677
53. Sugimoto, H., LeBleu, V. S., Bosukonda, D., Keck, P., Taduri, G., Bechtel, W., Okada, H., Carlson, W., Jr., Bey, P., Rusckowski, M., Tampe, B., Tampe, D., Kanasaki, K., Zeisberg, M., and Kalluri, R. (2012) Activin-like kinase 3 is important for kidney regeneration and reversal of fibrosis. *Nat. Med.* **18,** 396–404
54. Spiekerkoetter, E., Tian, X., Cai, J., Hopper, R. K., Sudheendra, D., Li, C. G., El-Bizri, N., Sawada, H., Haghighat, R., Chan, R., Haghighat, L., de Jesus Perez, V., Wang, L., Reddy, S., Zhao, M., Bernstein, D., Solow-Cordero, D. E., Beachy, P. A., Wandless, T. J., Ten Dijke, P., and Rabinovitch, M. (2013) FK506 activates BMPR2, rescues endothelial dysfunction, and reverses pulmonary hypertension. *J. Clin. Investig.* **123,** 3600–3613